# Small Unmanned Aircraft Thermal Infrared Imaging System to Identify Soybean Drought Tolerant Varieties (1879)

**Introduction**: During the course of the project two major projects were undertaken 1) Assessment of sudden death syndrome in soybean through multispectral broadband remote sensing aboard small unmanned aerial systems; and 2) Remote thermal infrared imaging for rapid screening of sudden death syndrome in soybean.

M.S. Student *Graduated: Nicholle Hatton*

Publications:

1. *Hatton, N.,* E. Menkeb, A. Sharda, D. Merwe and W. Schapaugh. 2019. Assessment of sudden death syndrome in soybean through multispectral broadband remote sensing aboard small unmanned aerial systems. Computers and Electronics in Agriculture. https://doi.org/10.1016/j.compag.2019.105094*
2. *Hatton, N.,* A. Sharda, W. Schapaugh and D. Merwe. 2020. Remote thermal infrared imaging for rapid screening of sudden death syndrome in soybean. Computers and Electronics in Agriculture. (Under 2nd Review)*

## Project 1: Assessment of sudden death syndrome in soybean through multispectral broadband remote sensing aboard small unmanned aerial systems

**Back ground**: sUAS aerial imagery has been utilized for years in precision agriculture. It is often combined or compared to ground-based systems for accuracy. Multispectral sensors are commonly used on sUAS platforms to detect canopy reflectance response through the generation of multispectral (MS) imagery. The imagery from multispectral sensors, commonly referred to as MS imagery, contain reflectance's response from selected visible to near infrared bands (blue/green/red/near infrared). The multispectral imagery generated from reflectance data gathered by sUAS-mounted broadband cameras provide useful information on photosynthesis and canopy energy balance. Overall, the capability of sensors aboard sUAS systems to provide data on-whole fields within a relatively short time, and the ability to use such data to conduct spatial analysis substantially expands research capabilities on topics such as plant health. (Gitelson & Merzlyak, 1998) (H. Zhang et al., 2013) (Lukas et al., 2016)

sUAS platforms have provided accurate data when directly compared to ground-based data, but few data have been collected on SDS using aerial remote sensing methods. To date, no studies have validated sUAS-based methods for accurate SDS detection. The utilization of sUAS to accurately assess SDS impacted fields would significantly reduce the time and cost of an evaluation compared with ground-based detection methods. The purpose of this research was to compare ground-based and aerial remote sensing methods for scoring of SDS, to determine if a novel index derived from multispectral sensors can be used for the assessment and quantification of SDS, and to assess if this index can be utilized for determination of maturity.

**Methods Utilized**: Soybean genotype plots were established in 2016 and 2017 crop seasons at the Kansas State University, Kansas River Valley Experiment Field outside of Rossville, Kansas (39.11852°, -95.92459°). The dominant soil type was a Eudora silt loam. The study area was selected because of a history of SDS impacted crops. No artificial inoculation of the crops with fungus was

required. No other major diseases were present at the site. Plots were planted on 12 May 2016 and 9 May 2017 into no-till corn stubble and pre-emergence herbicides were applied to prevent early season weed growth. Post-emergence applications of herbicide and manual removal were conducted to control weeds throughout the season. Irrigation was applied throughout the growing season to maintain adequate soil moisture and to help increase the severity of SDS. Maturity was recorded on all plots as the number of days after 31 August when 95% of the pods on the plants had reached mature color. Plots were harvested on 29 September 2016 and 4 October 2017.

Genotypes planted included a Nested Association Mapping population (NAM) consisting of 140 F5 derived lines from a cross between IA 3023 by LD00-3309 along with checks and experimental lines, for a total of 160 entries. Check plots included susceptible and resistant varieties. Some resistant varieties maintained a SDS score of 0. All 160 entries were planted in a randomized complete block design with four replications making a total of 640 plots. Each plot consisted of two rows which were 3.8 m long with 0.76 m row spacing. Among 160 entries, 16 entries were check varieties, which will be henceforth referred to as checks and check plots. The check plots were varieties with known SDS susceptibility and provided a benchmark to compare SDS for the remaining entries under consideration during this study. SDS resistant checks from maturity groups three and four were LD06-7862, Ripley, and LS09-1920. SDS susceptible checks from maturity groups three and four were Morgan and Spencer. Fields were fertilized to ensure no nutrient deficient symptoms occurred.

Ground-based measurements were collected on each plot from near canopy closure to the R7 growth stage (Fehr & Caviness, 1977), using two Ocean Optics USB2000 hyperspectral spectrometers (Ocean Optics, Largo, Florida, USA) mounted on a monopod to collect reflectance measurements from 350-1027 nm in increments of 0.38 nm. Data was collected on cloud-free days between 10 a.m. and 2 p.m. to limit solar effects

SDS ratings were taken on all plots at the R6 growth stage of the plants (Fehr et al., 1971). R6 refers to a growth stage with pod cavity filled, seeds just reaching full size. R6 has been designated for SDS scoring because symptom expression tends to be the best developed at this stage. All plots in 2016 and 2017 were scored for disease severity (Ds) on the scale of 1-9 based on foliar symptoms (Table 1) and disease incidence (Di) from 0-100% in 5% increments based on the amount of the plot that expressed foliar symptoms (Schmidt, 2007). Scoring was performed on 31 August 2016 and 6 September 2017 by the same individual to reduce as much variability as possible. Disease index or SDS score (Dx) was established by Equation 1 (Nijti et al., 2001) and will range from zero to 100.

**Table 1 - SDS severity scoring guidelines (adapted from Schmidt (2007))**

| Score | Description of Symptoms |
|---|---|
| 1 | 1-10% of leaf surface chlorotic, OR 1-5% necrotic |
| 2 | 10-20% of leaf surface chlorotic, OR 6-10% necrotic |
| 3 | 20-40% of leaf surface chlorotic, OR 11-20% necrotic |
| 4 | 40-60% of leaf surface chlorotic, OR 21-40% necrotic |
| 5 | Greater than 60% of leaf surface chlorotic, OR greater than 40% necrotic |
| 6 | Premature leaf drop up to 1/3 defoliation |

| | |
|---|---|
| 7 | Premature leaf drop up to 2/3 defoliation |
| 8 | Premature leaf drop GREATER than 2/3 defoliation |
| 9 | Premature death |

$$D_x = \frac{D_i * D_s}{9} \qquad \text{Equation 1}$$

Where:

Dx = SDS score or disease index

Di = Disease incidence

Ds = Disease severity

An IRIS+ multirotor (3D Robotics, Berkley, California, USA) and Ritewing Zephyr 3 (Rightwing Rc LLC, Apache Junction, Arizona, USA) fixed wing with a 47-inch wingspan sUAS were used as aerial platforms to mount spectral sensors and collect aerial imagery. The fixed wing had a designed endurance of 30 minutes flight with a payload of up to 400 g; whereas multirotor was designed for approximately five minutes of flight time with a similar payload. A modified Sony Alpha 5100 camera (Sony Corporation, Tokyo, Japan), converted to detect blue (B), green (G) and near infrared (NIR) bands (Arrow Consulting LLC, Manhattan, Kansas, USA), was utilized with the fixed-wing platform in 2016 and on the multirotor in 2017 to collect aerial imagery. The camera was modified by removal of the NIR blocking filter and installing a combination of purpose-designed band pass and notch filters that block visible red light from 570-690 mm, and near infrared above 780 nm. The installed filters, in combination with the Bayer array filter that is fused to the sensor and normally selects light wavelengths appropriately for B, G and R photosites on the sensor, resulted in overlapping B and G bands spanning 400-570 nm, and one NIR band (derived from native R photosites) spanning the transition of visible red edge to near infrared from 690-780 nm. Blocking near infrared light above 780 nm is necessary to avoid confounding responses to near infrared light in the B and G photosites. The camera was manually programmed, and settings were maintained for all flights. Camera settings were ISO 100, 1/4000 sec shutter speed, and f2.8. No spectral calibration of the images occurred during image capture.

The PI (pigment index), was derived by subtracting the GNDVI from the BNDVI (KSURF Invention Disclosure No. 2016-010, 2016). PI assesses reflectance from blue, green, and NIR regions captured with a modified broadband camera to assess plant stress (Equation 4). PI changes with the changing ratios of carotenoids to chlorophylls. Increased ratios of carotenoids to chlorophylls indicate stress conditions in the plant, or other physiological conditions that lead to changes in chlorophyll: carotenoid ratios, such as the normal progression through growth stages. Low PI values can be a sign of high concentrations of carotenoids, resulting from plant stress.

It was hypothesized that the introduction of stress and reduction of photosynthetic potential in plants suffering from SDS will result in lowered PI-values. To test this hypothesis, an experimental field of soybean with varied levels of SDS was assessed to determine the degree of correlation between SDS and PI values. As symptoms of SDS progress, the plant is unable to photosynthesize

at the same rate as healthy plants. The reduction of photosynthesis causes an increase in the blue light reflected. PI reduction due to stress and reduced photosynthetic activity are apparent in early and late stages of disease progression.

$$GNDVI = \frac{R_{NIR} - R_{Green}}{R_{NIR} + R_{Green}} \quad \text{Equation 2}$$

$$BNDVI = \frac{R_{NIR} - R_{Blue}}{R_{NIR} + R_{Blue}} \quad \text{Equation 3}$$

Where

$R_{NIR}$ = Reflectance in NIR (700-1200nm)

$R_{Blue}$ = Reflectance in blue (400-500 nm)

$R_{Green}$ = Reflectance in green (500-600 nm)

$$PI = BNDVI - GNDVI \quad \text{Equation 4}$$

Agisoft Photoscan Professional (Ver. 1.2.6, Agisoft LLC, St. Petersburg, Russia) generated an orthomosaic using weighted average values of all pixel reflectance values from individual photos. Ground reference panels were used for geometric correction and accuracy of the orthomosaic. The orthomosaic was then processed in ArcGIS 10.3 (ArcMap 10.4.1, Esri, Redlands, California, USA) to calculate GNDVI, BNDVI, and PI (Equations 2, 3 and 4). The spatial analysis tool was used to calculate and convert the orthomosaic into GNDVI, BDNVI, and PI maps of the field. The maps were generated with a color gradient of green to red indicating high to low vegetative index values, **Error! Reference source not found.**. Transects (approximately 3.8min length) were established through the approximate center of each row to extract and determine average GNDVI, BNDVI and PI for each plot.

**Results**:

Significant ($p \leq 0.01$) correlations between PI and SDS scores were observed within the 2016 check plots with aerial imagery and ground-based spectrometer data. Aerial and ground-based spectrometer data explained 90 and 73% of the variation in SDS scores of the check plots, respectively (Table 2). The increased accuracy and reduced variability from aerial to ground-based data could be accounted for as the broad band sensor covers the range of the carotenoid response while the GNDVI component of the ground-based PI fall outside the range of the carotenoid response. The broader wavelength range used in each channel of the broad band sensor results in complete coverage of the carotenoid response (Figure 1). Broadband camera bands overlap on the fringes of each band ensuring that the entire blue and green bands are covered while the spectrometer only accounts for a small portion of the blue and green bands. The ground-based GNDVI does not fall in the range of the carotenoid response however the BNDVI remain in the response range. Reassessment of the GNDVI to include wavelengths with in the carotenoid response (485 nm and 515 nm) was done to see if this would improve the ground-based results. These results showed the adjusted GNDVI ($P=0.2265$) and PI ($P=0.0641$) to both not be statistically significant. Thus, the greater accuracy of the aerial system to identify SDS justified the

exclusion of the ground-based unit for the 2017 season in favor of using only aerial imagery. Aerial systems can provide breeders, farmers and service providers a means to more rapidly assess SDS at relevant spatial scales.

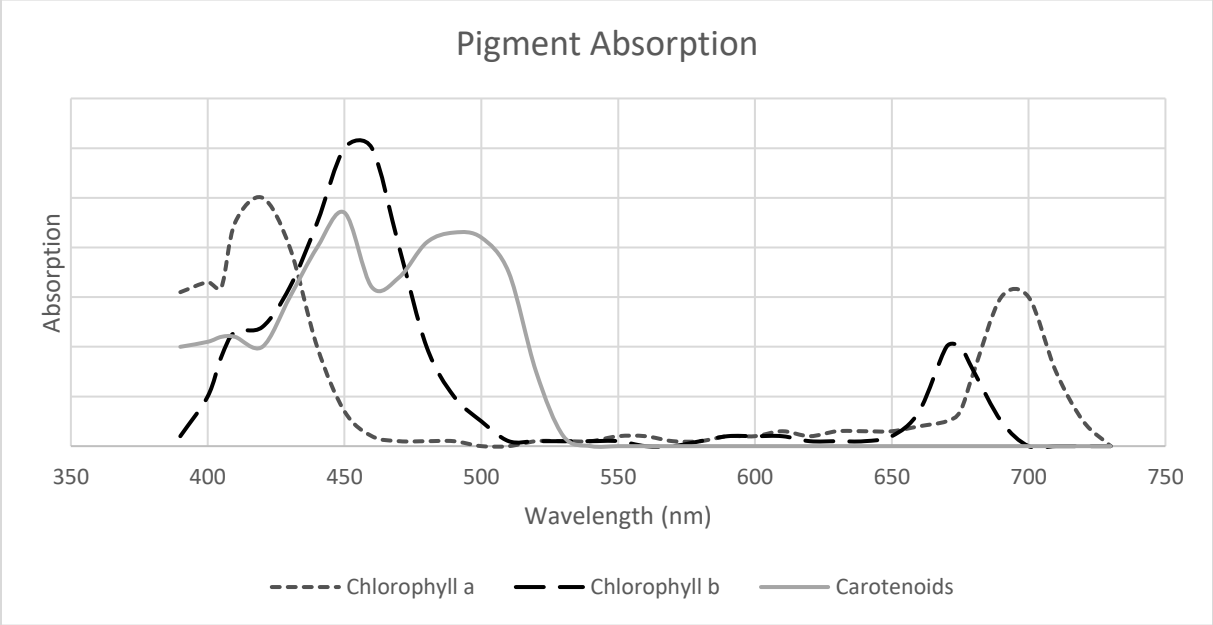


**Figure 1 - Absorption bands of Chlorophyll a and b, and carotenoids.**

An additional factor that may play a role in improved accuracy when using aerial systems is the shorter duration of data collection. sUAS missions took considerably less time to collect data (average flight time of approximately 11 minutes) compared to ground-based systems (average four hours) for the same area. During short duration aerial flights there were less changes in environmental factors that could influence data quality, including temperature, solar angle, wind, and cloud cover as compared to the several hours needed to complete ground-based surveys.

Table 2 – Aerial and ground-based data comparison. R2 given for SDS score, severity, and incidence of check plots. Statistically significant values ($P < 0.01$) are noted by an asterisk (n=10)

| Variable | Aerial | Ground-Based |
|---|---|---|
| **SDS score** | 0.90* | 0.73* |
| **Severity** | 0.80* | 0.74* |
| **Incidence** | 0.80* | 0.63* |

PI exhibited the highest correlation with SDS scores among the three indices (GNDVI, BNDVI, and PI) for FD2 and FD3 (Table 3). GNDVI was not significantly correlated with SDS scores for either FD2 or FD3. BNDVI was significantly correlated with SDS on both dates, but the correlations (-0.36 and -0.35 for FD2 and FD3) were considerably lower than when using PI (-0.79 and -0.72 for FD2 and FD3).

Table 3 - Spearman's Rho of GNDVI, BNDVI, and PI with SDS score for FD2 and FD3. Statistically significant values ($P < 0.001$) are noted given an asterisk (n=160)

| DAY | GNDVI | BNDVI | PI |
|---|---|---|---|
| FD2 | -0.08 | -0.36* | -0.79* |
| FD3 | -0.07 | -0.35* | -0.72* |

Breeding programs will eliminate the genotypes with the highest response to SDS to increase resistance to SDS. Since SDS infection was low in 2016, the 2017 data was used to assess the ability of PI, BNDVI and GNDVI to identify plots with high SDS for elimination. The top 50% of the entries based on SDS scores were compared with the bottom 50% of the entries based on PI values to quantify the percentage of susceptible entries identified correctly using PI. SDS scores for the top 50% of the entries with the most severe SDS ranged from 30 to 94. The lowest 50% of the entries based on the PI from FD2 recognized 80% of top 50% of the entries with the most severe SDS. The lowest 50% of the entries based on the PI from FD3 recognized 79% of top 50% of the entries with the most severe SDS. Using BNDVI as the selection criteria correctly identified 69% and 73% of the top entries for FD2 and FD3, respectively. GNDVI only identified 54% and 64% of the most severely infested entries for FD2 and FD3, respectively. The comparison of results showed that PI could better characterize SDS than BNDVI and GNDVI when the aerial imagery was collected when SDS leaf symptoms were visible and before plant senescence. Overall, the results indicated PI can assist both breeders and potentially farmers in identifying high SDS infected soybean with high confidence on a spatial scale.

**Conclusions**: This study exhibited that aerial SDS assessment using a sUAS data collection method was comparable to ground-based data collection methods, and SDS is quantifiable from aerial platforms over a whole field. PI acts as an indicator of SDS indirectly correlating to SDS score, incidence and severity. PI derived using aerial imagery showed a strong negative correlation to the SDS scores for checks and high scoring SDS plots in 2016. Analysis of PI from aerial imagery as a detector of SDS provided results comparable to ground-based system with the aerial system showing a stronger relationship with less variability. Decreased variability in the aerial scores was explained by the ability for the broadband sensor to cover the range of the carotenoid response. Overall, the aerial imaging systems can provide field data in a relatively short amount of time with potentially minimal environmental variability and improved SDS estimation though PI as compared to the ground-based collected data.

Aerial PI also presented a strong correlation over a whole field in the 2017 growing season. Individual components of SDS score, severity, and incidence were analyzed to assess their strength as measurements of SDS. SDS severity maintained the least variability and highest correlation to PI across the 2017 data including SDS score. Additionally, ability of PI to detect SDS severity is a promising indicator for SDS identification across all field sizes including large farming operations. Further, PI presented a strong correlation to the maturity of plots. PI not only acts as an indicator of plant health but also plant senescence and maturity.

In soybean breeding programs, time available for phenotypic evaluation is one of the largest restraints in breeding new lines. The ability to use sUAS to collect data over a larger area in a short amount of time presents opportunities to evaluate a greater number of breeding lines in a given year. The estimated SDS values can then be used as the basis of selection, with at least the potential of

eliminating the more susceptible genotypes. The use of aerial imagery and PI could potentially be most useful in early generation screening of large amounts of breeding material, and subsequent evaluation of selected material by breeders to ensure the proper characterization of the material to SDS. Future studies will include an early assessment of SDS to determine if SDS is detectable through broadband multispectral imagery before visible symptoms appear. Future work will include determining if PI can detect SDS before any visible symptoms are seen as well as if PI can be used for detection of other diseases impacting farmers across America.

## Project 2: Assessment of sudden death syndrome in soybean through multispectral broadband remote sensing aboard small unmanned aerial systems

**Background**: The plant experiences stress-induced nutrient deficiencies, caused by the initial root infection, in the early stages of SDS. Worsening of SDS will eventually prohibit normal plant functions, namely evapotranspiration, to a point where the plant can no longer maintain homeostasis. These diseased plants should exhibit higher canopy temperatures than healthy plants, which could provide a proxy for measuring SDS severity.

Thermal infrared (TIR) imagery measures an objects emitted radiation. The emitted radiation of an object can be used to derive the canopy temperature. Changes in plant canopy temperature can be caused by stress, disease, nutrient deficiencies and water stress. Mapping crop canopy temperature uses TIR imagery (Alves & Pereira, 2000; Ayeneh, van Ginkel et al., 2002; J. A. J. Berni, Zarco-Tejada et al., 2009; Espinoza et al., 2017; Luo et al., 2018; X. Wang et al., 2010). TIR imagery is also used in the estimation of biomass (Gunawardena & Fernando, 2016; Maimaitijiang et al., 2017; Wooster et al., 2013), prediction of yields (Guan et al., 2017; Hecker, Smith et al., 2013; Leroux et al., 2016), assessment of fruit and crop quality (Berdugo et al., 2014; Sepulcre-Cantó et al., 2013; Sepulcre-Cantó et al., 2007; Zhao et al., 2005) and assessment of water stress (Hong et al., 2019). Thermal evaluation of SDS for the determination of disease symptoms or severity has not yet been attempted. However, work from Berdugo et al. (2014), Calderón et al. (2014a), Chaerle et al. (2004), A. Mahlein et al. (2012), and Oerke et al., 2006 assess diseased and healthy plant temperatures under greenhouse conditions. These studies demonstrate that as early as two days after inoculation, temperatures of diseased plants can increase by 2$^{0}$C or more as the disease progresses (Chaerle et al., 2004; Oerke et al., 2006). Further work by Calderón et al. (2013) and De Carolis et al. (1974) used thermal imaging to assess early detection of diseases in olive trees and rice. Both studies demonstrated that early disease detection is possible when using elevated canopy temperatures as the main indicator between diseased and healthy plants (Calderón et al., 2013; De Carolis et al., 1974).

The aim of this case study was to 1) demonstrate that SDS infected soybean exhibit elevated canopy temperatures, and 2) explore the temporal effects of disease progression using thermal imagery acquired by a small unmanned aerial system (sUAS).

**Methods:** An approach to compare SDS infected plants to healthy plants was established through the development of this case study. Naturally infected soybean over a typical growing season served as the sample population for this study. The relationship between canopy temperature and SDS score is assessed over several days after canopy closure is reached.

Study Area

The study area was located at the Kansas State University, Kansas River Valley Experiment Field outside Rossville, KS (39.11852°, -95.92459°) and was selected for its prevalent SDS history. The dominant soil in the field is Eudora silt loam. Irrigation was applied throughout the growing season to maintain adequate soil moisture and to help increase the severity of SDS.

All plots had maturity and SDS ratings collected. Maturity was recorded as the number of days following 31 August when 95% of the pods on the plants had reached mature color. SDS ratings were taken at the R6 growth stage of the plants (Fehr et al., 1971).

The experiment consisted of a Nested Association Mapping (NAM) population comprised of 140 F5 derived lines from a cross between IA3023 and LD00-3309 along with checks for yield, and agronomic traits and susceptible and resistant checks for resistance to Soybean Sudden Death Syndrome (SDS), for 160 entries. The experiment used a randomized complete block design with four replications consisting of two-row plots 3.8 m long with 0.76 m between rows, and henceforth will be mentioned as plots for aerial imagery analysis. The field was planted on 9 May 2017 into corn stubble and application of pre-emergence herbicide prevented early season weed growth. Postemergence herbicide applications and hand weeding controlled weeds throughout the season. SDS was scored on two criteria, severity and incidence. Severity (Ds) addresses the severity of the SDS infection based foliar symptoms, on a scale of 0-9, as shown in **Error! Reference source not found.**. Scoring occurred at growth stage R6 on 6 September 2017. R6 is the growth stage where the seedpod cavity is filled, and seeds have reached full size. R6 is designated as an appropriate stage of development for SDS scoring due to the expression of the disease symptoms (Schmidt, 2007).

Aerial imagery was acquired using a sUAS coupled with a thermal camera designed for sUAS use. The IRIS+ (3DR, Berkeley, California, USA) in combination with a FLIR VUE Pro R 19 mm thermal camera (FLIR Systems, Wilsonville, Oregon, USA) captured imagery for this study. The thermal camera measured spectral bands from 7.5-13.5 μm. Note: Results from this study may not be similar for cameras with wider lenses.

Flights occurred four times toward the end of the season on 28 August, 3 September, 8 September, and 13 September. Flights began at 12:00 p.m. on each day. A flight altitude 77 m above ground level (AGL) allowed a flight time of 7 minutes covering an area of about 1.8 hectares with a spatial resolution of 6.89 cm/pixel. Side lap was set to 75% while front-to-back overlap was set to 85% to achieve a one-second camera trigger interval. The sUAS was programmed to fly at a ground speed of 3 m/s. Based on the preliminary studies conducted with different ground speeds, the 3 m/s ground speed provided images with minimal blur.

Reference panels were instrumented to measure actual temperature and develop a temperature versus sensor digital response regressions function to calibrate and derive canopy temperatures from images. A canopy calibration is necessary as the thermal camera alone has an accuracy of +/- 5°C. Temperatures of reference panels were measured using surface-mounted thermistors (ON-930-44033, Omega Engineering Inc., Stamford, Connecticut, USA) with a measurement accuracy of ±0.1°C. Reference panels were painted black, grey, and white, while a water bath served as a fourth reference. The different colored panels and water bath provided different temperature gradients for canopy temperature calibration. Laboratory experiments showed that reference panels have uniform temperature across the surface. Air temperature were taken from the Mesonet network

(http://mesonet.k-state.edu/about/network/) that operates a weather station located at 39.086 latitude, -95.926 longitude, about 400 m from the experimental field. The weather stationed recorded air temperature with an accuracy of ±0.3°C @ 0 to 40°C. Weather conditions for all flights were clear and atmospherically stable with minimal wind.

Data processing

Sixteen plots each with high (SDS score of 25 and over), medium (SDS score of 8-17), and low (SDS score of 0-5) SDS were randomly selected for comparison for a total of 48 plots. Independent images from each day were analyzed in FLIR Tools (FLIR Systems, Wilsonville, Oregon, USA) to derive the canopy temperature of each plot. Temperature was derived from the emitted radiation of the plot captured by the sensor. FLIR Tools used the target's emissivity, distance from the sensor to object (flight altitude AGL), relative humidity, and atmospheric temperature to derive the temperature. Emissivity was set at 0.94 nm (Guoquan & Zhengzhi, 1993; Rubio et al., 1997). Distance, relative humidity, and atmospheric temperature were set in camera settings in the field each day based on the daily conditions. Derived plot temperature was taken as the average temperature for that plot on a given day. The plots had complete canopy closure with no soil visible in the background; therefore, the area of each plot was drawn to derive average plot canopy temperature. The canopy temperature (Tc) was calculated for each plot for each day as the average canopy temperature over seven images (five consecutive images with the target plot visible in the middle during a single pass of the flight and one left and one right image) (Figure 2 and Table 4). Averaging over seven images eliminated bias that could occur due to changes in the angle between the canopy and sensor.

Table 4 – Example average canopy temperature and standard deviation for two plots of each low, medium and high SDS from 3 September flight. Air temperature during flight was 28.6ºC. The LT and RT represents image of the plot on the left and right side of the sUAS during flight.

| SDS SCORE | PLOT | IMG 1 (ºC) | IMG 2 (ºC) | IMG 3 (ºC) | IMG 4 (ºC) | IMG 5 (ºC) | SIDE LT (ºC) | SIDE RT (ºC) | AVG (ºC) | STD DIV |
|---|---|---|---|---|---|---|---|---|---|---|
| **0.0** | 302 | 25.4 | 25.4 | 25.3 | 25.3 | 25.4 | 26.1 | 23.8 | 25.4 | 0.09 |
| **0.6** | 4 | 24.7 | 24.8 | 24.9 | 24.3 | 24.6 | 26.7 | 23.7 | 24.7 | 0.23 |
| **10.0** | 24 | 26.3 | 26.4 | 26.4 | 25.6 | 25.8 | 28.3 | 25.9 | 26.1 | 0.38 |
| **11.1** | 101 | 26.0 | 26.2 | 26.4 | 26.3 | 26.3 | 27.7 | 25.3 | 26.2 | 0.15 |
| **85.0** | 165 | 28.2 | 27.9 | 28.5 | 28.1 | 28.4 | 29.3 | 27.8 | 28.2 | 0.23 |
| **100.0** | 121 | 28.4 | 27.7 | 27.9 | 28.4 | 28.4 | 28.6 | 27.6 | 28.2 | 0.34 |

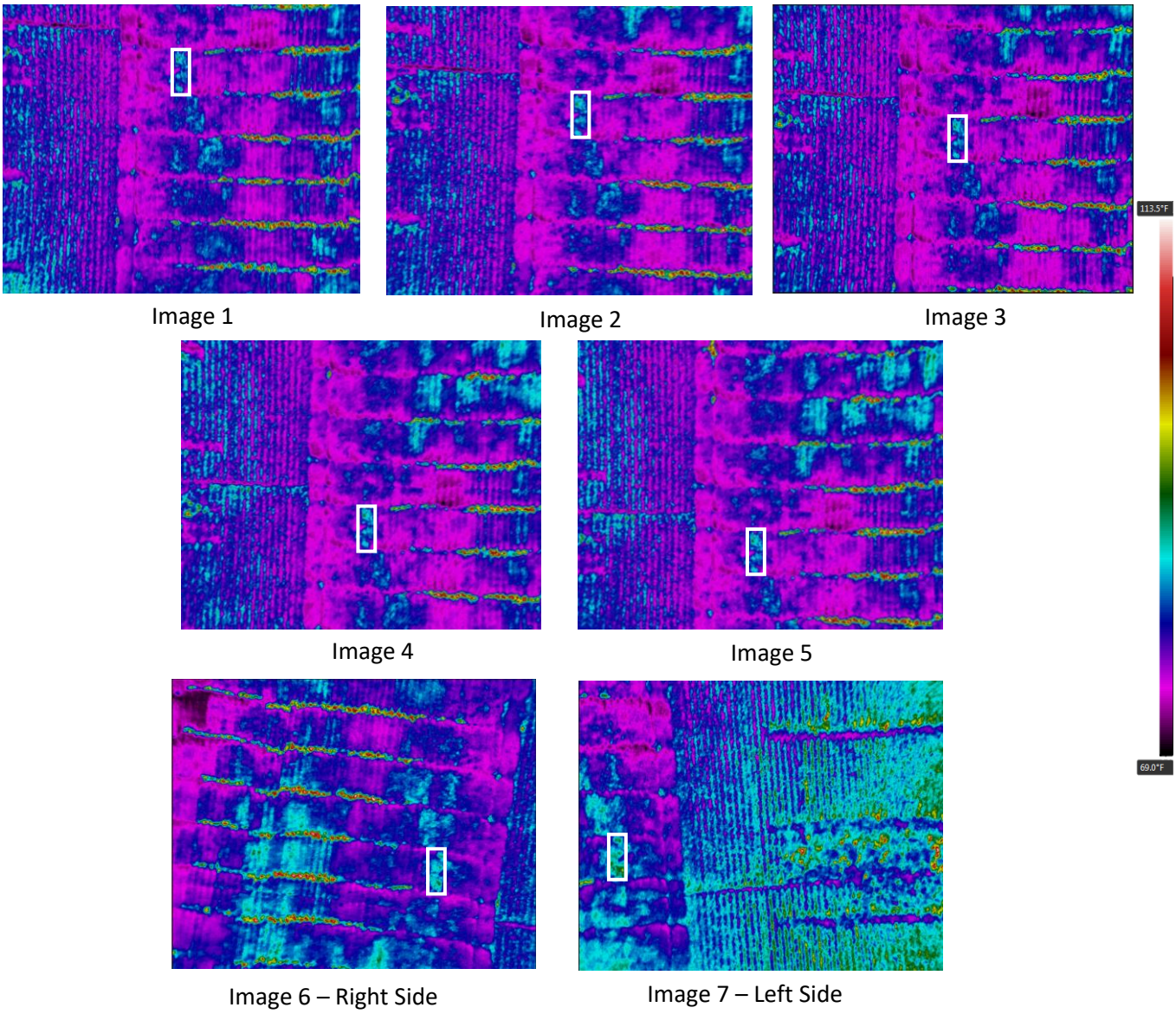


Figure 2 – Example sequence of image selection for calculation of average canopy temperature. Plot 121 circled to show relative position in each image.

**Results**: Average canopy temperature for all four flying dates varied between 21.2º C and 27.8º C, with standard deviation varying from 1.03º C to 1.53º C. Table 2 shows an example of the canopy temperature averaging over seven images. Six plots (two low, two medium, and two high SDS scores) were chosen in the example. These results indicated the TIR sensor had a consistent response to canopy emittance for the series of images taken over the plots. It is also evident from the results that the canopy temperature was consistent when capturing canopy emitted radiation from different angles during multiple passes of the flight. Overall, these results are specifically observed for 19 mm thermal camera, and results may be different when using a 13 mm or a 9mm thermal camera. Temperature difference was compared to SDS scoring for each day flown to assess the relationship between temperature and SDS prevalence for each day. Each study period presented significance ($P < 0.0001$) in the relationship between temperature and SDS score, incidence, and

severity. Figure 3 displays the temperature difference of each day compared to SDS score. Spearman's rho correlation increased throughout the growing season with a moderate correlation observed for 28 August ($\varrho$ = 0.5344) and the strongest correlation observed for 13 September ($\varrho$ = 0.7404). Temperature difference exhibited a positive correlation to the SDS score for each day, with larger temperature differences observed in the plots with higher SDS scores. A steady increase in Tc-Ta is seen from 28 August to 13 September. This difference becomes more pronounced in the plants with high SDS infection. Plots with low SDS infection maintain canopy temperatures below the air temperature. On 3 September highly infected plant canopy temperatures begin approaching the air temperature. By 8 September most highly and moderately infected plots have canopy temperatures above the air temperature.

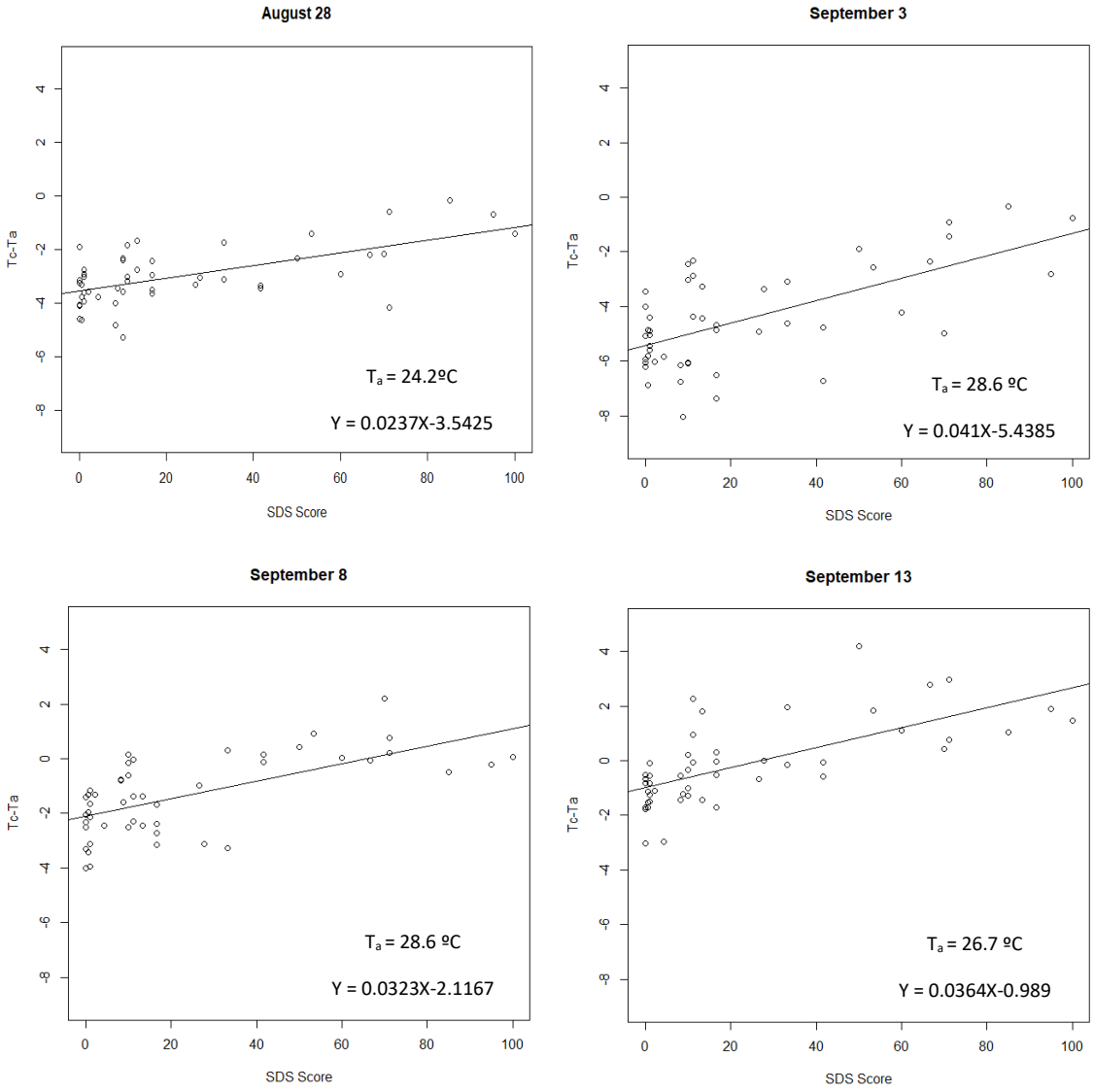


Figure 3 - SDS score to Tc-Ta (temperature difference) for each day of UAS flight. Equation for line of fit and Spearman's rho ($\varrho$) are given for each plot. Correlation coefficients that were statistically significant ($P<0.0001$) are indicated by an asterisk.

Strong correlations were observed between temperature difference and SDS severity and incidence for each of the four sUAS flights (Figure 44 and Figure 5). Both severity and incidence displayed similar statistical significance and correlation to temperature difference for a given day. As evident in Figure 4 and 5, both severity and incidence for 3 September displayed a low temperature difference compared to other days of flight including 28. The general trend for each day demonstrates that higher temperature reflected greater extent of SDS infection in plants within a plot. The overall increase in correlation demonstrates the progression of the disease over the growing season. SDS scores were taken on 6 September when visual symptoms were reaching maximum expression. However, affected plots began showing symptoms two weeks earlier than the SDS rating were measured (i.e. SDS scoring). 28 August exhibited few visual symptoms of SDS but exhibited higher temperatures due to stress caused by SDS. Early detection of SDS infection could lead to increased yields if mitigation steps could be implemented before visual symptoms develop.

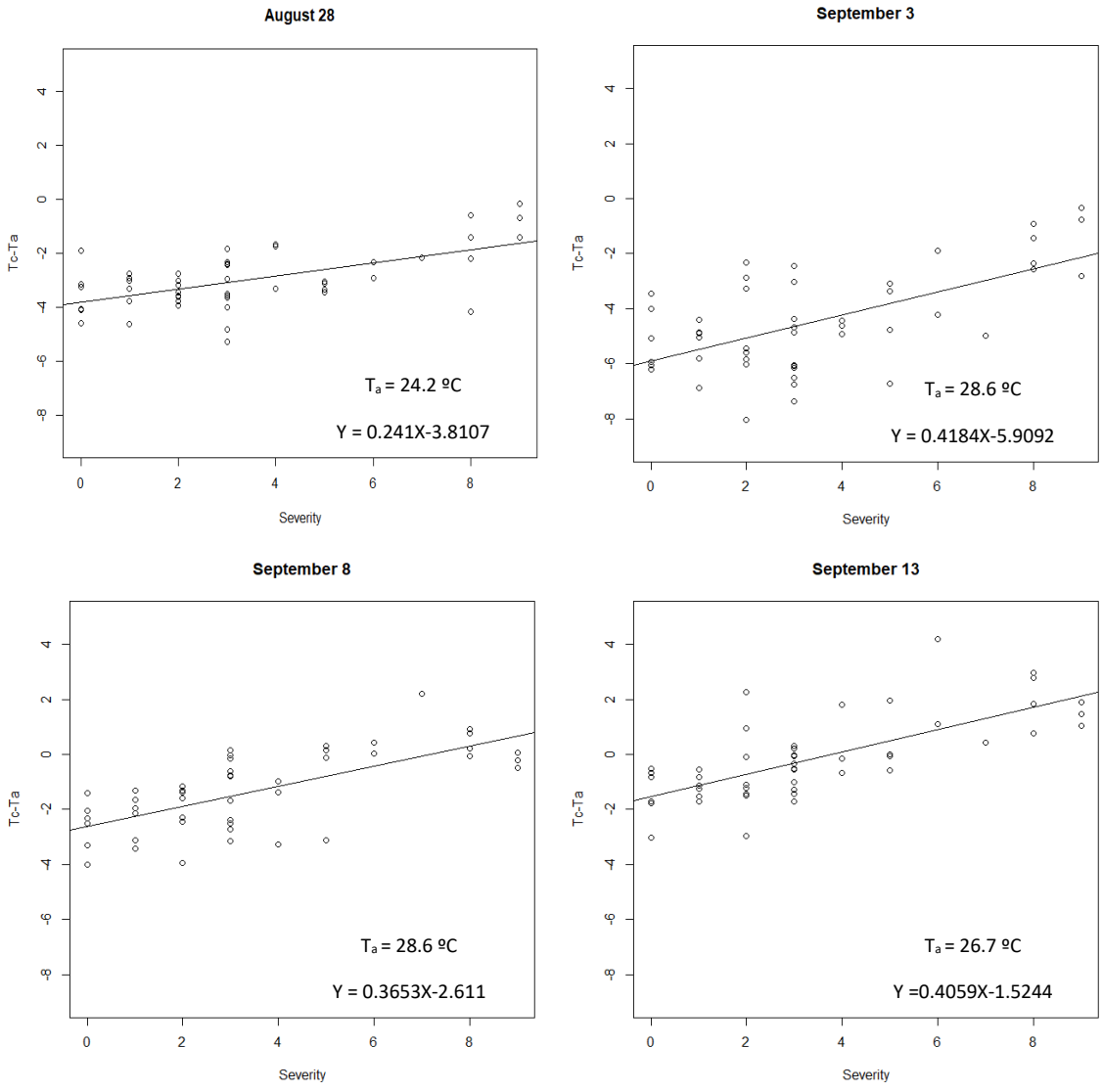

**Figure 4 - Severity of infection to Tc-Ta (temperature difference for each day of UAS flight. Equation for line of fit and Spearman's rho (ϱ) are given for each plot. Correlation coefficients that were statistically significant (P<0.0001) are indicated by an asterisk.**

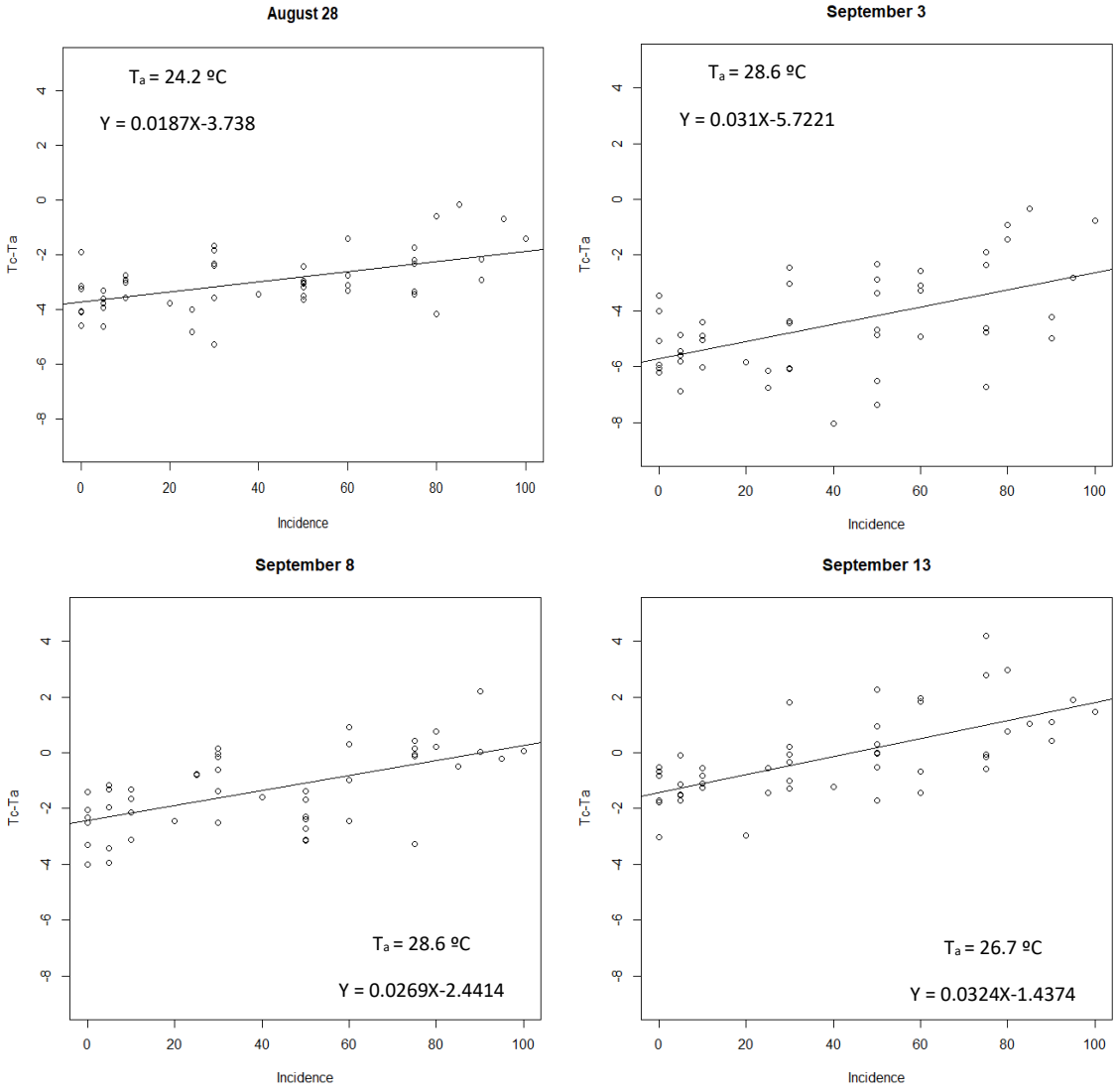


**Figure 5 - Incidence of infection to Tc-Ta (temperature difference) for each day of UAS flight. Equation for line of fit and Spearman's rho (ϱ) are given for each plot. Correlation coefficients that statistically significant (P < 0.0001) are indicated by an asterisk.**

**Conclusions**: Previous studies showed that thermal assessment of disease was possible through aerial platforms. This case study demonstrated that an infield assessment of soybean SDS using a TIR camera and sUAS system was possible. Correlations with temperature difference and SDS score increased throughout the growing season. Correlations with disease incidence and severity also increased through the growing season with the largest correlations toward the end of the seed fill

period Overall assessment of incidence displayed the highest relationship in correlation over the days flown while severity maintained a similar relationship. Severity of SDS infection is the most practical predictor of SDS for large application use because of its high correlation and easy application.

This case study exhibits the potential use of TIR remote sensing for detection of SDS in soybean. While correlations at the beginning of the flight period were moderate, they have potential to act as predictors to SDS within a field and give preliminary indications of the disease before visual symptoms appear. Future studies will expand this research to assess disease over an entire field and determine when the earliest that definable SDS symptoms are present.

**Consolidated References**:

**References Project II**


Alves, I., & Pereira, L. S. (2000). Non-water-stressed baselines for irrigation scheduling with infrared thermometers: A new approach. Irrigation Science, 19(2), 101-106.

Ayeneh, A., van Ginkel, M., Reynolds, M. P., & Ammar, K. (2002). Comparison of leaf, spike, peduncle and canopy temperature depression in wheat under heat stress. Field Crops Research, 79(2), 173-184. 10.1016/S0378-4290(02)00138-7

Berdugo, C. A., Zito, R., Paulus, S., & Mahlein, A. -. (2014). Fusion of sensor data for the detection and differentiation of plant diseases in cucumber. Plant Pathology, 63(6), 1344-1356. 10.1111/ppa.12219

Berni, J. A. J., Zarco-Tejada, P., Suarez, L., & Fereres, E. (2009). Thermal and narrowband multispectral remote sensing for vegetation monitoring from an unmanned aerial vehicle.(author abstract)(technical report). IEEE Transactions on Geoscience and Remote Sensing, 47(3), 722. 10.1109/TGRS.2008.2010457

Calderón, R., Navas-Cortés, J. A., Lucena, C., & Zarco-Tejada, P. (2013). High- resolution airborne hyperspectral and thermal imagery for early detection of verticillium wilt of olive using fluorescence, temperature and narrow- band spectral indices. Remote Sensing of Environment, 139, 231-245. 10.1016/j.rse.2013.07.031

Calderón, R., Montes-Borrego, M., Landa, B., Navas-Cortés, J., & Zarco-Tejada, P. (2014). Detection of downy mildew of opium poppy using high- resolution multi-spectral and thermal imagery acquired with an unmanned aerial vehicle. Precision Agriculture, 15(6), 639-661. 10.1007/s11119-014-9360-y

Chaerle, L., Hagenbeek, D., De Bruyne, E., Valcke, R., & Van, D. S. (2004). Thermal and chlorophyll- fluorescence imaging distinguish plant- pathogen interactions at an early stage. Plant and Cell Physiology, 45(7), 887-896. 10.1093/pcp/pch097

Chong, S. -., Hildebrand, K. K., Luo, Y., Myers, O., Indorante, S. J., Kazakevicius, A., & Russin, J. (2005). Mapping soybean sudden death syndrome as related to yield and soil/site properties. Soil and Tillage Research, 84(1), 101-107. 10.1016/j.still.2004.09.001

Cui, D., Zhang, Q., Li, M., Slaminko, T., & Hartman, G. L. (2014). A method for determining the severity of sudden death syndrome in soybeans. Transactions of the ASABE, 57(2), 671-678. 10.13031/trans.57.9837

De Carolis, C., Baldi, G., Galli de Paratesi, S., & Lechi, G. M. (1974). Thermal behaviour of some rice fields affected by a yellows-type disease.2, 1161-1170.

Espinoza, C. Z., Khot, L. R., Sankaran, S., & Jacoby, P. W. (2017). High resolution multispectral and thermal remote sensing-based water stress assessment in subsurface irrigated grapevines. Remote Sensing, 9(9)10.3390/rs9090961

Fehr, W. R., Caviness, C. F., Burmood, D. T., & Pennington, J. S. (1971). Stage of development descriptions for soybeans, glycine max (L.) merrill. Crop Sci, 11, 929-931.

Guan, K., Wu, J., Kimball, J. S., Anderson, M. C., Frolking, S., Li, B., . . . Lobell, D. B. (2017). The shared and unique values of optical, fluorescence, thermal and microwave satellite data for estimating large-scale crop yields. Remote Sensing of Environment, 199, 333-349. 10.1016/j.rse.2017.06.043

Gunawardena, A., & Fernando, T. (2016). Use of optical, thermal IR and radar satellite data to estimate above ground biomass in montane forests of sri lanka. Paper presented at the 37th Asian Conference on Remote Sensing, ACRS 2016, , 2 945-951.

Guoquan, D., & Zhengzhi, L. (1993). The apparent emissivity of vegetation canopies. International Journal of Remote Sensing, 14(1), 183-188. 10.1080/01431169308904329

Hartman, G. L., Sinclair, J. B., & Rupe, J. C. (1999). Sudden death syndrome. Compendium of soybean diseases (Forth ed., pp. 37-38). St. Paul, Minnesota: APS Press.

Hecker, C. A., Smith, T. E. L., Luz, R. D., & Wooster, M. J. (2013). Thermal infrared spectroscopy in the laboratory and field in support of land surface remote sensing10.1007/978-94-007-6639-6_3

Hong, M., Bremer, D. J., & van der Merwe, D. (2019). Thermal Imaging Detects Early Drought Stress in Turfgrass Utilizing Small Unmanned Aircraft Systems. Agrosystems, Geosciences & Enviroment, 2(1), 0. doi: 10.2134/age2019.04.0028

Leroux, L., Baron, C., Zoungrana, B., Traore, S. B., Lo Seen, D., & Begue, A. (2016). Crop monitoring using vegetation and thermal indices for yield estimates: Case study of a rainfed cereal in semi-arid west africa. IEEE Journal of Selected Topics in Applied Earth Observations and Remote Sensing, 9(1), 347-362. 10.1109/JSTARS.2015.2501343

Luo, D., Jin, H., Marchenko, S. S., & Romanovsky, V. E. (2018). Difference between near-surface air, land surface and ground surface temperatures and their influences on the frozen ground on the qinghai-tibet plateau. Geoderma, 312, 74-85. 10.1016/j.geoderma.2017.09.037

Mahlein, A., Oerke, E., Steiner, U., & Dehne, H. (2012). Recent advances in sensing plant diseases for precision crop protection. European Journal of Plant Pathology; Published in Cooperation with the European Foundation for Plant Pathology, 133(1), 197-209. 10.1007/s10658-011-9878-z

Maimaitijiang, M., Ghulam, A., Sidike, P., Hartling, S., Maimaitiyiming, M., Peterson, K., . . . Fritschi, F. (2017). Unmanned aerial system (UAS)-based phenotyping of soybean using multi-sensor data

fusion and extreme learning machine. ISPRS Journal of Photogrammetry and Remote Sensing, 134, 43-58. 10.1016/j.isprsjprs.2017.10.011

Manage soybean risks, SDS and SCN with ILeVO. (2016). Retrieved from http://www.crossroadstoday.com/story/34649679/manage-soybean-risks-sds-and-scn-with-ilevo

Nijti, V., Johnson, J., Torto, T., Gray, L., & Lightfoot, D. (2001). Inoculum rate influences selection for field resistance to soybean sudden death syndrome in the greenhouse. Crop Science, 41(6), 1726-1731. 10.2135/cropsci2001.1726

Oerke, E. C., Steiner, U., Dehne, H., & Lindenthal, M. (2006). Thermal imaging of cucumber leaves affected by downy mildew and environmental conditions. Journal of Experimental Botany; J.Exp.Bot., 57(9), 2121-2132. 10.1093/jxb/erj170

Roy, K. W., Rupe, J. C., Hershman, D. E., & Abney, T. S. (1997). Sudden death syndrome of soybean. Plant Disease, 81(10), 1100-1111.

Rubio, E., Caselles, V., & Badenas, C. (1997). Emissivity measurements of several soils and vegetation types in the 8– 14, μm wave band: Analysis of two field methods. Remote Sensing of Environment, 59(3), 490-521. 10.1016/S0034-4257(96)00123-X

Schmidt, C. (2007). SIUC method of SDS scoring Southern Illinois University Carbondale.

Sepulcre-Cantó, G., Gellens-Meulenberghs, F., Arboleda, A., Duveiller, G., De Wit, A., Eerens, H., . . . Defourny, P. (2013). Estimating crop- specific evapotranspiration using remote- sensing imagery at various spatial resolutions for improving crop growth modelling. International Journal of Remote Sensing, 34(9-10), 3274-3288. 10.1080/01431161.2012.716911

Sepulcre-Cantó, G., Zarco-Tejada, P. J., Jiménez-Muñoz, J. C., Sobrino, J. A., Soriano, M. A., Fereres, E., . . . Pastor, M. (2007). Monitoring yield and fruit quality parameters in open-canopy tree crops under water stress. implications for ASTER. Remote Sensing of Environment, 107(3), 455-470. 10.1016/j.rse.2006.09.014

Shrivastava, S., Singh, S. K., & Hooda, D. S. (2015). Color sensing and image processing-based automatic soybean plant foliar disease severity detection and estimation. Multimedia Tools and Applications, 74(24), 11467-11484. 10.1007/s11042-014-2239-0

Tang, E., Hill, C. B., & Hartman, G. L. (2010). Carbon utilization profiles of fusarium virguliforme isolates. Canadian Journal of Microbiology, 56(12), 979-986. 10.1139/W10-085

Wang, X., Yang, W., Wheaton, A., Cooley, N., & Moran, B. (2010). Automated canopy temperature estimation via infrared thermography: A first step towards automated plant water stress monitoring. Computers and Electronics in Agriculture, 73(1), 74-83. 10.1016/j.compag.2010.04.007

Westphal, A., Xing, L., Abney, T. S., & Shaner, G. (2006). Diseases of soybean: Sudden death syndrome. Purdue Extension BP-58-W, (4)

Wooster, M. J., Roberts, G., Smith, A. M. S., Johnston, J., Freeborn, P., Amici, S., . . . Hudak, A. T. (2013). Thermal remote sensing of active vegetation fires and biomass burning events10.1007/978-94-007-6639-6_18

Xing, L., & Westphal, A. (2009). Effects of crop rotation of soybean with corn on severity of sudden death syndrome and population densities of heterodera glycines in naturally infested soil. Field Crops Research, 112(1), 107-117. 10.1016/j.fcr.2009.02.008

Zhang, H., Lan, Y., Suh, C. P. -., Westbrook, J., Clint Hoffmann, W., Yang, C., & Huang, Y. (2013). Fusion of remotely sensed data from airborne and ground-based sensors to enhance detection of cotton plants. Computers and Electronics in Agriculture, 93, 55-59. 10.1016/j.compag.2013.02.001

Zhao, C., Liu, L., Wang, J., Huang, W., Song, X., & Li, C. (2005). Predicting grain protein content of winter wheat using remote sensing data based on nitrogen status and water stress. International Journal of Applied Earth Observations and Geoinformation, 7(1), 1-9. 10.1016/j.jag.2004.10.002

**References Project I**

Anderson, J., Akond, M., Kassem, M. A., Meksem, K., & Kantartzi, S. K. (2015). Quantitative trait loci underlying resistance to sudden death syndrome (SDS) in MD96-5722 by 'Spencer' recombinant inbred line population of soybean. 3 Biotech, 5(2), 203-210. doi:10.1007/s13205-014-0211-3

Bajwa, S. G., Rupe, J. C., & Mason, J. (2017). Soybean disease monitoring with leaf reflectance. Remote Sensing, 9(2) doi:10.3390/rs9020127

Bartlett, M.S., (1978). Nearest neighbor models in the analysis of field experiments. J. R. Stat. Soc., Ser. B 40:147-174.

Bendig, J., Bolten, A., Bennertz, S., Broscheit, J., Eichfuss, S., & Bareth, G. (2014). Estimating biomass of barley using crop surface models (CSMs) derived from UAV-based RGB imaging. Remote Sensing, 6(11), 10395-10412. doi:10.3390/rs61110395

Bybordi, S., & Reggiani, L. (2015). (2015). Drones in agriculture: Applications and outlook. Paper presented at the Dipartimento Di Elettroniva Informazione e Bioingegneria,

Calderón, R., Montes-Borrego, M., Landa, B. B., Navas-Cortés, J. A., & Zarco-Tejada, P. J. (2014). Detection of downy mildew of opium poppy using high-resolution multi-spectral and thermal imagery acquired with an unmanned aerial vehicle. Precision Agriculture, 15(6), 639-661. doi:10.1007/s11119-014-9360-y

Campomanes, F. P., V., Silapan, J. R., & Blanco, A. C. (2015). Building footprint extraction using LiDAR data and spectral indices from aerial imagery. Paper presented at the ACRS 2015 - 36th Asian Conference on Remote Sensing: Fostering Resilient Growth in Asia, Proceedings,

Castaldi, F., Pelosi, F., Pascucci, S., & Casa, R. (2017). Assessing the potential of images from unmanned aerial vehicles (UAV) to support herbicide patch spraying in maize. Precision Agriculture, 18(1), 76-94. doi:10.1007/s11119-016-9468-3

Chappelle, E. W., Kim, M. S., & Mcmurtrey, J. E. (1992). Ratio analysis of reflectance spectra ( RARS): An algorithm for the remote estimation of the concentrations of chlorophyll A, chlorophyll B, and carotenoids in soybean leaves. Remote Sensing of Environment, 39(3), 239-247. doi:10.1016/0034-4257(92)90089-3

Chong, S. -., Hildebrand, K. K., Luo, Y., Myers, O., Indorante, S. J., Kazakevicius, A., & Russin, J. (2005). Mapping soybean sudden death syndrome as related to yield and soil/site properties. Soil and Tillage Research, 84(1), 101-107. doi:10.1016/j.still.2004.09.001

Collings, S., & Caccetta, P. (2011). On the generation of broad-scale hyperspectral ground reflectance mosaics from aerial and ground-based observations. International Journal of Image and Data Fusion, 2(3), 237-253. doi:10.1080/19479832.2010.551523

Corti, M., Cavalli, D., Cabassi, G., Vigoni, A., Degano, L., & Marino Gallina, P. (2018). Application of a low-cost camera on a UAV to estimate maize nitrogen-related variables. Precision Agriculture, doi:10.1007/s11119-018-9609-y

Cui, D., Zhang, Q., Li, M., Slaminko, T., & Hartman, G. L. (2014). A method for determining the severity of sudden death syndrome in soybeans. Transactions of the ASABE, 57(2), 671-678. doi:10.13031/trans.57.9837

d'Oleire-Oltmanns, S., Marzolff, I., Peter, K. D., Ries, J. B., & Hssaïne, A. A. (2011). (2011). Monitoring soil erosion in the souss basin, morocco, with a multiscale object-based remote sensing approach using UAV and satellite data. Paper presented at the 1st World Sustainability Forum, Basel, Switzerland.

Fehr, W. R., & Caviness, C. F. (1977). Stage of soybean development. (Special Report No. 80). Ames, Iowa: Iowa State Iniversity.

Fehr, W. R., Caviness, C. F., Burmood, D. T., & Pennington, J. S. (1971). Stage of development descriptions for soybeans, glycine max (L.) merrill. Crop Sci, 11, 929-931.

Feng, W., Shen, W., He, L., Duan, J., Guo, B., Li, Y., … Guo, T. (2016). Improved remote sensing detection of wheat powdery mildew using dual-green vegetation indices. Precision Agriculture, 17(5), 608–627. doi: 10.1007/s11119-016-9440-2

Gitelson, A. A., Kaufman, Y. J., & Merzlyak, M. N. (1996). Use of a green channel in remote sensing of global vegetation from EOS- MODIS. Remote Sensing of Environment, 58(3), 289-298. doi:10.1016/S0034-4257(96)00072-7

Gitelson, A. A., & Merzlyak, M. N. (1998). Remote sensing of chlorophyll concentration in higher plant leaves. Advances in Space Research, 22(5), 689-692. doi:10.1016/S0273-1177(97)01133-2

Gómez-Candón, D., De Castro, A., & López-Granados, F. (2014). Assessing the accuracy of mosaics from unmanned aerial vehicle (UAV) imagery for precision agriculture purposes in wheat. Precision Agriculture, 15(1), 44-56. doi:10.1007/s11119-013-9335-4

Gómez-Candón, D., Virlet, N., Labbé, S., Jolivot, A., & Regnard, J. -. (2016). Field phenotyping of water stress at tree scale by UAV-sensed imagery: New insights for thermal acquisition and calibration. Precision Agriculture, 17(6), 786-800. doi:10.1007/s11119-016-9449-6

Granados-Ramírez, R., Reyna-Trujillo, T., Gómez-Rodríguez, G., & Soria-Ruiz, J. (2004). Analysis of NOAA-AVHRR-NDVI images for crops monitoring. International Journal of Remote Sensing, 25(9), 1615-1627. doi:10.1080/0143116031000156855

Hartman, G. L., Sinclair, J. B., & Rupe, J. C. (1999). Sudden death syndrome. Compendium of soybean diseases (Forth ed., pp. 37-38). St. Paul, Minnesota: APS Press.

Heliospectra. (2014). LED light spectrum 101: Absorption spectra. Retrieved from https://www.heliospectra.com/articles/led-light-spectrum-101-absorption-spectra/

Herrmann, Ittai & K Vosberg, Steven & Ravindran, Prabu & Singh, Aditya & Chang, Hao-Xun & I Id, Martin & Chilvers, Martin & Conley, Shawn & Townsend, Philip. (2018). Leaf and Canopy Level Detection of Fusarium Virguliforme (Sudden Death Syndrome) in Soybean. Remote Sensing. 10. 10.3390/rs10030426.

Hodecker, B. E. R., Pita-Barbosa, A., de Barros, N. F., & Merchant, A. (2018). Water availability preceding long-term drought defines the tolerance of eucalyptus to water restriction. New Forests, 49(2), 173-195. doi:10.1007/s11056-017-9612-6

Huang, Y., Lan, Y., Ge, Y., Hoffmann, W. C., & Thomson, S. J. (2010). Spatial modeling and variability analysis for modeling and prediction of soil and crop canopy coverage using multispectral imagery from an airborne remote sensing system. Transactions of the ASABE, 53(4), 1321-1329.

Kaleita, A. L. (2006). Fusion of remotely sensed imagery and minimal ground sampling for soil moisture mapping Digital Repository @ Iowa State University.

Kang, L., Ji, C. Y., Kim, S. H., Ke, Q., Park, S. -., Kim, H. S., . . . Kwak, S. -. (2017). Suppression of the ß-carotene hydroxylase gene increases ß-carotene content and tolerance to abiotic stress in transgenic sweetpotato plants. Plant Physiology and Biochemistry, 117, 24-33. doi:10.1016/j.plaphy.2017.05.017

Kim, S. H., Ahn, Y. O., Ahn, M., Lee, H., & Kwak, S. (2012). Down- regulation of β- carotene hydroxylase increases β- carotene and total carotenoids enhancing salt stress tolerance in transgenic cultured cells of sweetpotato. Phytochemistry, 74, 69-78. doi:10.1016/j.phytochem.2011.11.003

Krienke, B., Ferguson, R. B., Schlemmer, M., Holland, K., Marx, D., & Eskridge, K. (2017). Using an unmanned aerial vehicle to evaluate nitrogen variability and height effect with an active crop canopy sensor. Precision Agriculture, 18(6), 900-915. doi:10.1007/s11119-017-9534-5

Liu, F., Qin, Q., & Zhan, Z. (2012). A novel dynamic stretching solution to eliminate saturation effect in NDVI and its application in drought monitoring. Chinese Geographical Science, 22(6), 683-694. doi:10.1007/s11769-012-0574-5

Lukas, V., Novák, J., Neudert, L., Svobodova, I., Rodriguez-Moreno, F., Edrees, M., & Kren, J. (2016). The combination of UAV survey and landsat imagery for monitoring of crop vigor in precision agriculture. Paper presented at the International Archives of the Photogrammetry, Remote Sensing and Spatial Information Sciences - ISPRS Archives, , 41 953-957. doi:10.5194/isprsarchives-XLI-B8-953-2016

Manage soybean risks, SDS and SCN with ILeVO. (2016). Retrieved from http://www.crossroadstoday.com/story/34649679/manage-soybean-risks-sds-and-scn-with-ilevo

McGwire, K. C., Weltz, M. A., Finzel, J. A., Morris, C. E., Fenstermaker, L. F., & McGraw, D. S. (2013). Multiscale assessment of green leaf cover in a semi-arid rangeland with a small unmanned aerial vehicle. International Journal of Remote Sensing, 34(5), 1615-1632. doi:10.1080/01431161.2012.723836

Mitchell, J. J., Glenn, N. F., Anderson, M. O., Hruska, R. C., Halford, A., Baun, C., & Nydegger, N. (2012). Unmanned aerial vehicle (UAV) hyperspectral remote sensing for dryland vegetation monitoring. Paper presented at the 2012 4th Workshop on Hyperspectral Image and Signal Processing, WHISPERS 2012, June 4, 2012 - June 7, ASD; et al.; EXELI S; Golden Way Scientific;

HySpex; Itres. doi:10.1109/WHISPERS.2012.6874315 Retrieved from http://dx.doi.org/10.1109/WHISPERS.2012.6874315

Ngaki, M. N., Wang, B., Sahu, B. B., Srivastava, S. K., Farooqi, M. S., Kambakam, S., . . . Bhattacharyya, M. K. (2016). Tanscriptomic study of the soybean-fusarium virguliforme interaction revealed a novel ankyrin-repeat containing defense gene, expression of whose during infection led to enhanced resistance to the fungal pathogen in transgenic soybean plants. PLoS ONE, 11(10) doi:10.1371/journal.pone.0163106

Nijti, V., Johnson, J., Torto, T., Gray, L., & Lightfoot, D. (2001). Inoculum rate influences selection for field resistance to soybean sudden death syndrome in the greenhouse. Crop Science, 41(6), 1726-1731. doi:10.2135/cropsci2001.1726

Overview: MIXED Procedure. (2010, April 30). Retrieved from https://support.sas.com/documentation/cdl/en/statug/63033/HTML/default/viewer.htm#statug_mixed_sect001.htmPhatak, A. (2004). A user-friendly guide to multivariate calibration and classificationtion, T. næs, T. isaksson, T. fearn, T. davies: Chichester: NIR publications. Chemometrics and Intelligent Laboratory Systems, 71(1), 79-81. doi:http://dx.doi.org/10.1016/j.chemolab.2003.12.010

Primicerio, J., Di Gennaro, S., Fiorillo, E., Genesio, L., Lugato, E., Matese, A., & Vaccari, F. (2012). A flexible unmanned aerial vehicle for precision agriculture. Precision Agriculture; an International Journal on Advances in Precision Agriculture, 13(4), 517-523. doi:10.1007/s11119-012-9257-6

Roy, K. W., Rupe, J. C., Hershman, D. E., & Abney, T. S. (1997). Sudden death syndrome of soybean. Plant Disease, 81(10), 1100-1111.

Salami, E., Barrado, C., & Pastor, E. (2014). UAV flight experiments applied to the remote sensing of vegetated areas. Remote Sensing, 6(11), 11051-11081. doi:10.3390/rs61111051

Sankaran, S., Khot, L. R., & Carter, A. H. (2015). Field-based crop phenotyping: Multispectral aerial imaging for evaluation of winter wheat emergence and spring stand. Computers and Electronics in Agriculture, 118, 372-379. doi:10.1016/j.compag.2015.09.001

Schmidt, C. (2007). SIUC method of SDS scoring Southern Illinois University Carbondale.

Tang, E., Hill, C. B., & Hartman, G. L. (2010). Carbon utilization profiles of fusarium virguliforme isolates. Canadian Journal of Microbiology, 56(12), 979-986. doi:10.1139/W10-085

Themistocleous, K., Papadavid, G., Christoforou, M., Agapiou, A., Andreou, K., Tsaltas, D., & Hadjimitsis, D. G. (2014). Use of remote sensing and UAV for the management of degraded ecosystems: The case study of overgrazing in randi forest, cyprus. Paper presented at the 2nd International Conference on Remote Sensing and Geoinformation of the Environment, RSCy 2014, April 7, 2014 - April 10, , 9229 et al.; Euro-agriwot; European Cooperation in Science and Technology (COST); Geosystems Hellas; Intergraph; Li-Cor. doi:10.1117/12.2069515 Retrieved from http://dx.doi.org/10.1117/12.2069515

Tucker, C. J., Vanpraet, C. L., Sharman, M. J., & Van Ittersum, G. (1985). Satellite remote sensing of total herbaceous biomass production in the senegalese sahel: 1980– 1984. Remote Sensing of Environment, 17(3), 233-249. doi:10.1016/0034-4257(85)90097-5

Van der Merwe, D. (2016). KSURF Invention Disclosure No. 2016-010. Manhattan. KS: Kansas State University.

Westphal, A., Xing, L., Abney, T. S., & Shaner, G. (2006). Diseases of soybean: Sudden death syndrome. Purdue Extension BP-58-W, (4)

Wrather, J. A., & Koenning, S. R. (2006). Estimates of disease effects on soybean yields in the united states 2003 to 2005. Journal of Nematology, 38(2), 173-180.

Xing, L., & Westphal, A. (2009). Effects of crop rotation of soybean with corn on severity of sudden death syndrome and population densities of heterodera glycines in naturally infested soil. Field Crops Research, 112(1), 107-117. doi:10.1016/j.fcr.2009.02.008

Zhang, C., & Kovacs, J. M. (2012). The application of small unmanned aerial systems for precision agriculture: A review. Precision Agriculture, 13(6), 693-712. doi:10.1007/s11119-012-9274-5

Zhang, H., Lan, Y., Suh, C. P. -., Westbrook, J., Clint Hoffmann, W., Yang, C., & Huang, Y. (2013). Fusion of remotely sensed data from airborne and ground-based sensors to enhance detection of cotton plants. Computers and Electronics in Agriculture, 93, 55-59. doi:10.1016/j.compag.2013.02.001